Supplemental Figure 1.

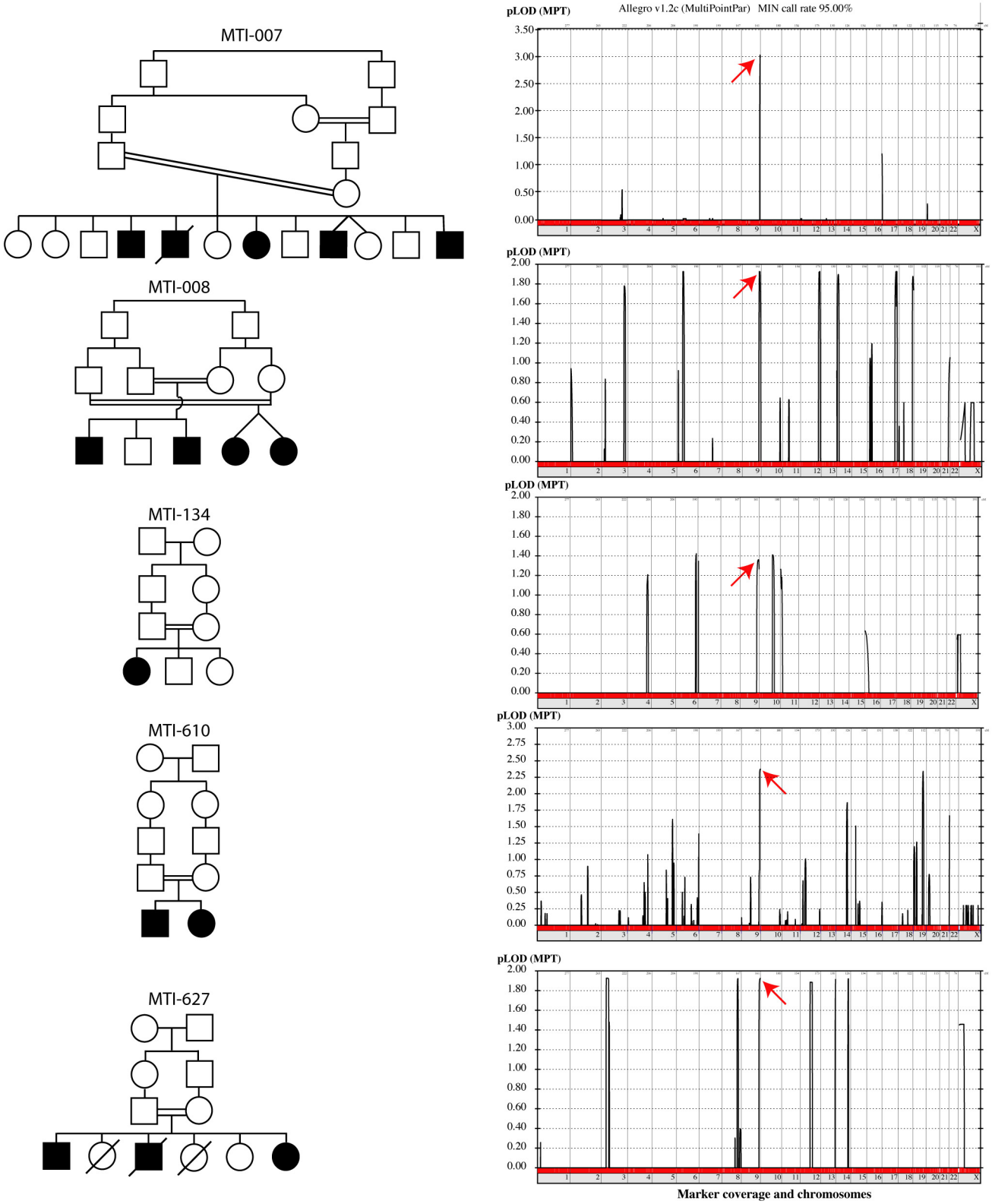

Supplemental Figure 1. Pedigrees and linkage plots for families used in this study. Left shows pedigrees. Double bar documents consanguinity. Males = square, female = circle, hashed line = deceased. All families have documented consanguinity. Right shows LOD score plots, with chromosome along x-axis, and multipoint plod along y-axis, as calculated by Allegro v1.2c. Note the peak at Chr. 9q term in all families included in this study.

Supplemental Figure 2.

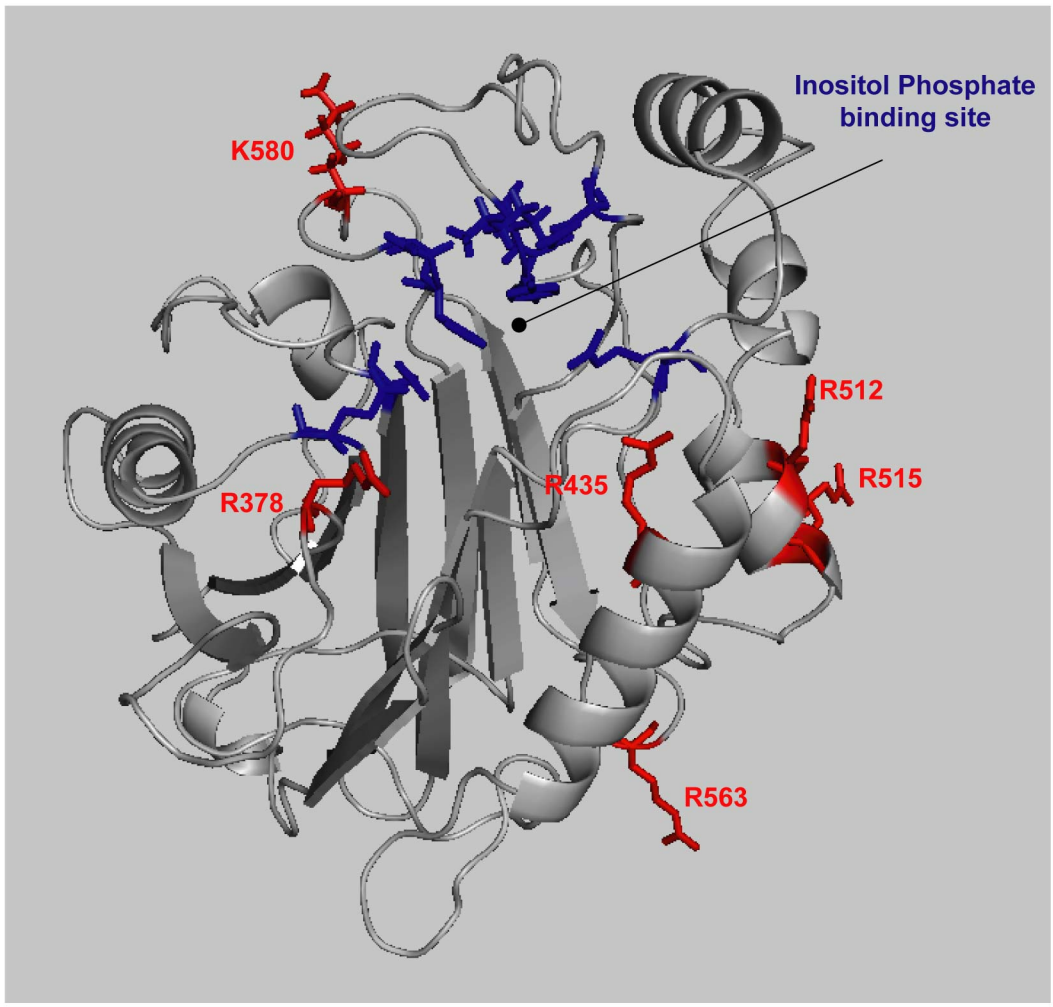

Supplemental Figure 2. Homology modeling of wild-type INPP5E using crystallized synaptojanin 5-phosphatase as a template. The inositol phosphate binding site is shown by black dot, with key resides mediating binding indicated in blue. The location of amino acids mutated in JS patients are indicated in red, and most are located in the face of the binding pocket.

Supplemental Figure 3.

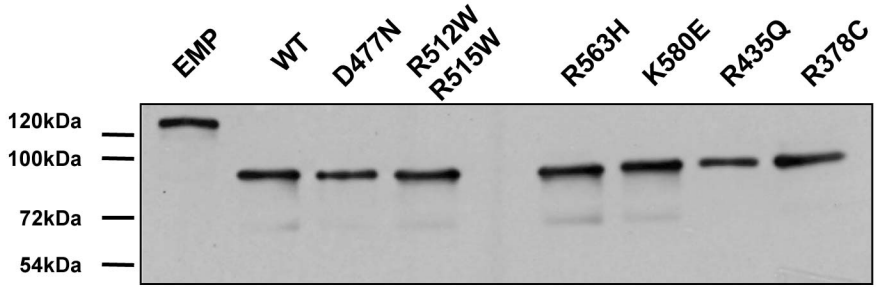

Supplemental Figure 3. Western blot using Myc antibody demonstrating comparable amounts of immunoprecipitated INPP5E for each corresponding patient mutation compared with positive and negative controls, used subsequently for enzymatic assays in Fig. 2.

Supplemental Figure 4.

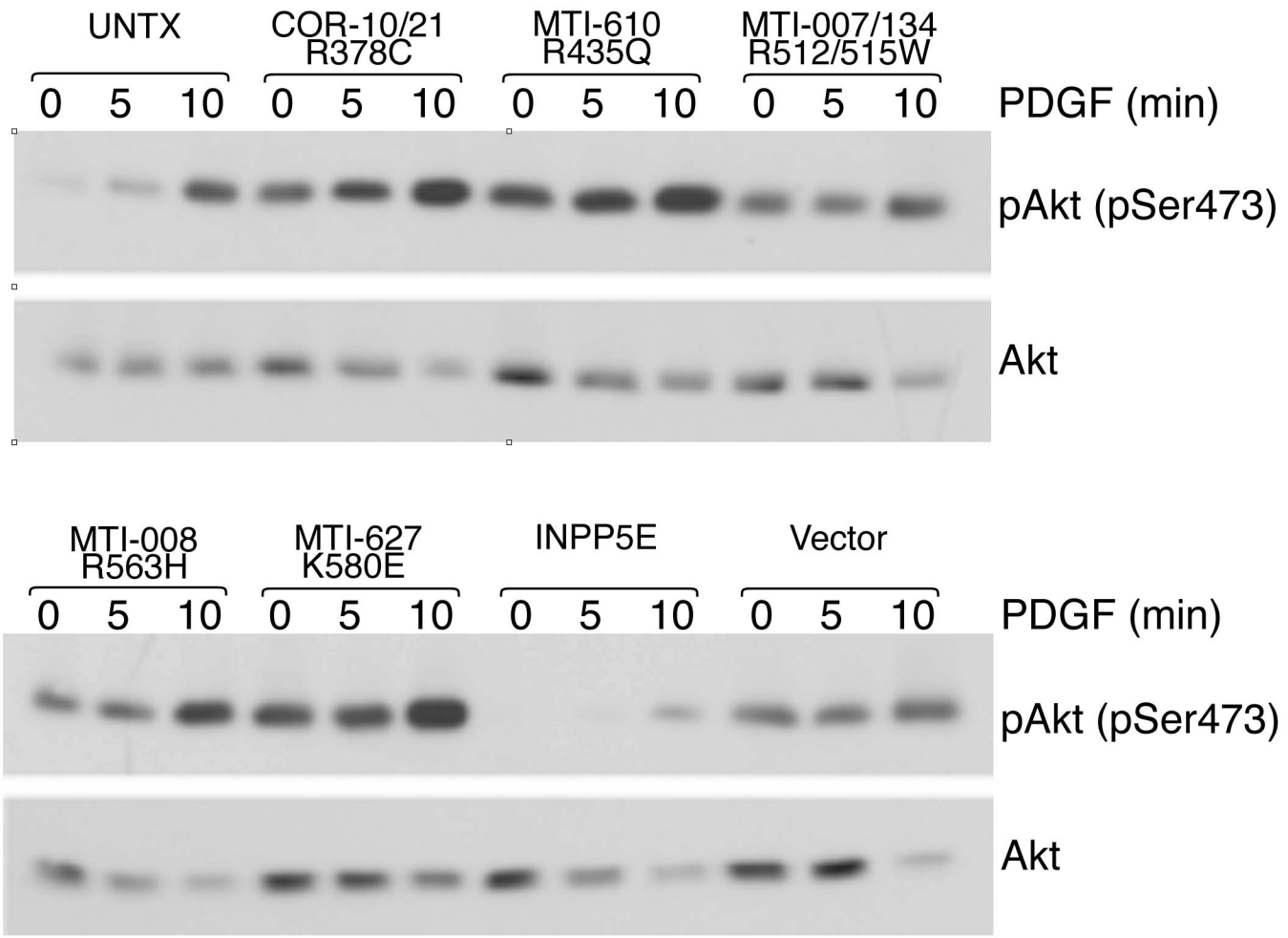

Supplemental Figure 4. INPP5E patient mutations fail to block Akt phosphorylation in response to PDGF stimulation. 293T cells were stably transfected to inducibly overexpress INPP5E cDNAs (untransfected, wildtype INPP5E, empty vector, or patient mutations). Cells were then induced with tetracycline, followed by PDGF stimulation. Total and phospho-Akt levels were assessed at 0, 5 and 10 minutes.

Supplemental Figure 5.

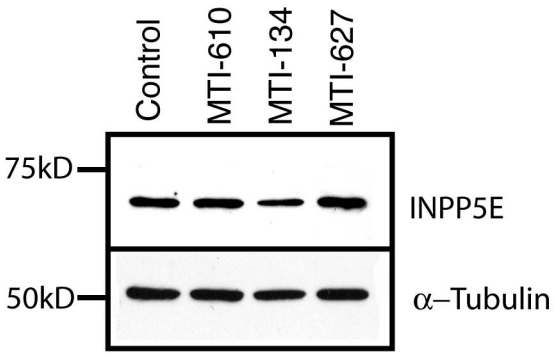

Supplemental Figure 5. Western blot using INPP5E antibody demonstrating comparable amounts of INPP5E expressed in growth-arrested fibroblasts from control vs. three different patients. α-Tubulin was used as a loading control.

Supplemental Figure 6.

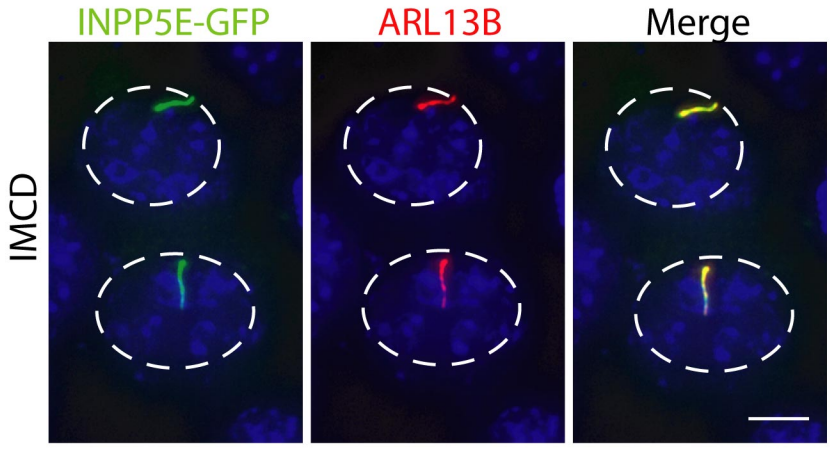

Supplemental Figure 6. Localization of transfected GFP-tagged INPP5E to primary cilia. Intramedullary collecting duct cells (IMCD) were transfected with GFP-tagged INPP5E, then fixed and stained for ARL13B to visualize cilia. ARL13B-positive cilia are also positive for INPP5E. Nuclei are circled, scale bar 5 um.

Supplemental Figure 7.

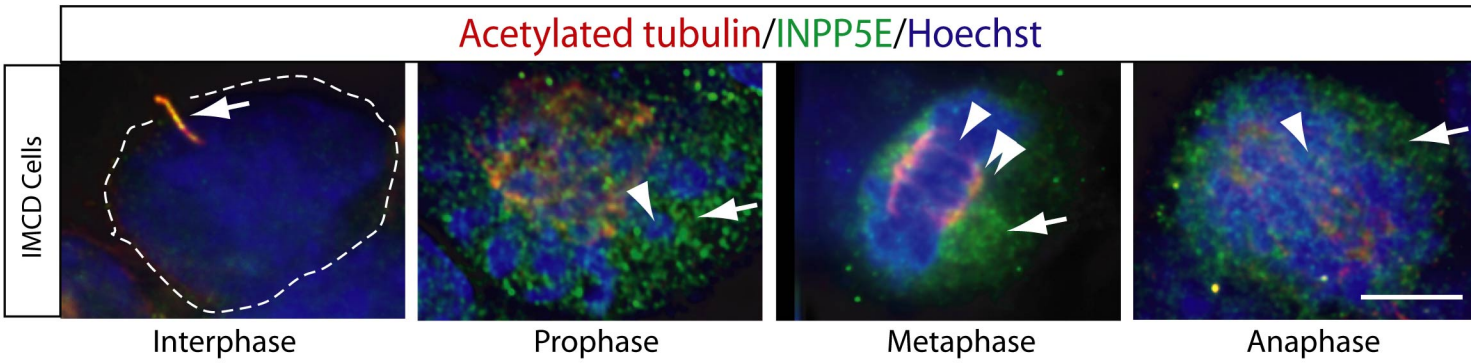

Supplemental Figure 7. INPP5E (green) localization at interphase compared with stages of mitosis in IMCD-3 cells, co-stained for acetylated tubulin (red) and Hoechst nuclei (blue). At interphase, a single cilium is apparent (arrow) and INPP5E shows localization to this site. During stages of mitosis, when the cilium has been reabsorbed, INPP5E shows cytoplasmic localization. Arrows = INPP5E localization. Arrowheads = condensed chromatin. Double arrowhead = spindle microtubules. Scale bar = 5 um.

Supplemental Figure 8.

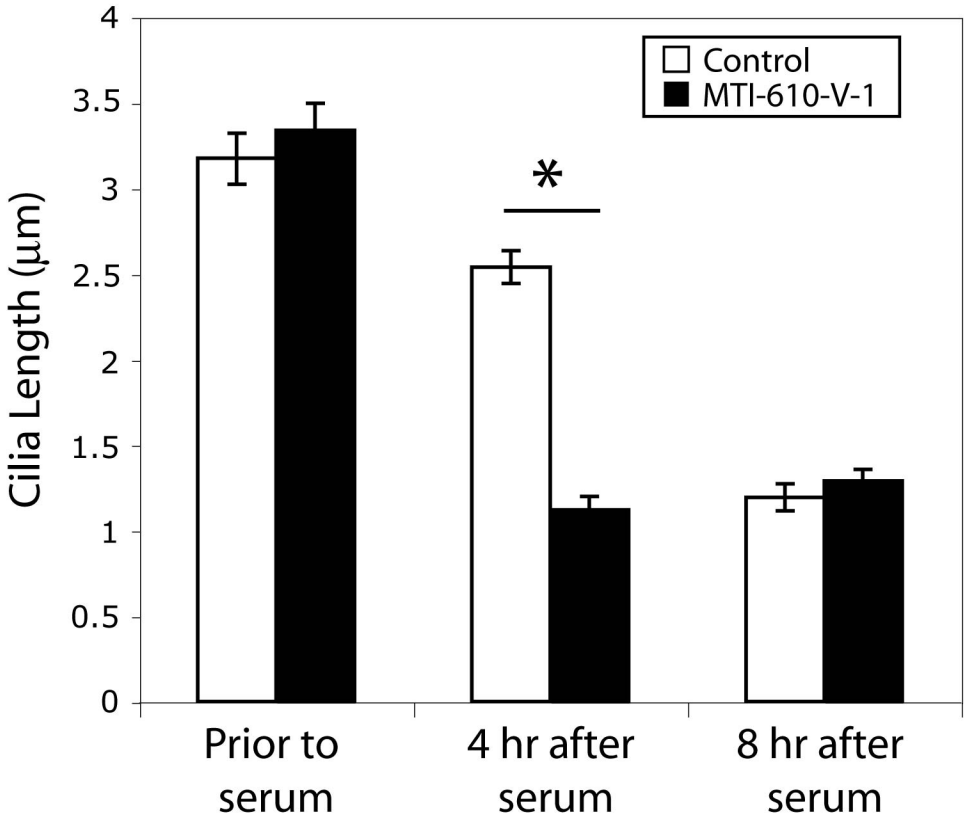

Supplemental Figure 8. Quantification of cilia length in control vs. MTI-610-V-1 primary fibroblasts. Serum was added at time = 0 hrs, and cilia length was assessed from x-y projection images at 0, 4 and 8 hrs. Cilia length was significantly reduced in mutant cells at 4 hrs, suggesting enhanced cilia lability in the absence of functioning INPP5E.

Supplemental Figure 9.

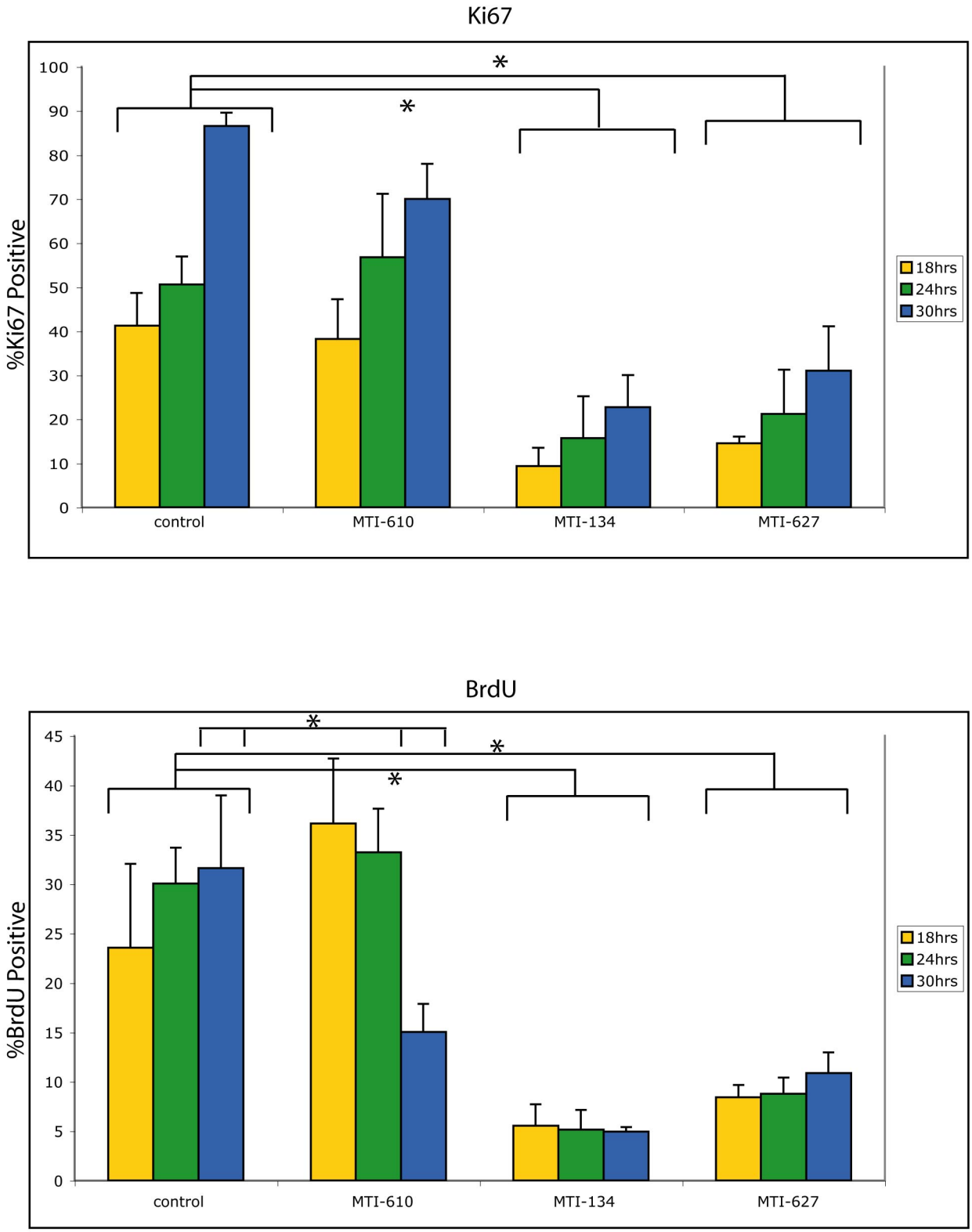

Supplemental Figure 9. Altered cell cycle dynamics in INPP5E-mutant samples. Growth-arrested subconfluent fibroblasts were assessed for cell cycle reentry based upon BrdU incorporation and Ki67 positivity, at various timepoints after 20% serum addition. MTI-134 and MTI-627 were significantly different from control for both parameters at all three timepoints, whereas MTI-610 was different only for BrdU incorporation at 30 hrs. * represents $p < 0.05$ paired comparison of one-way ANOVA.

Supplemental Figure 10.

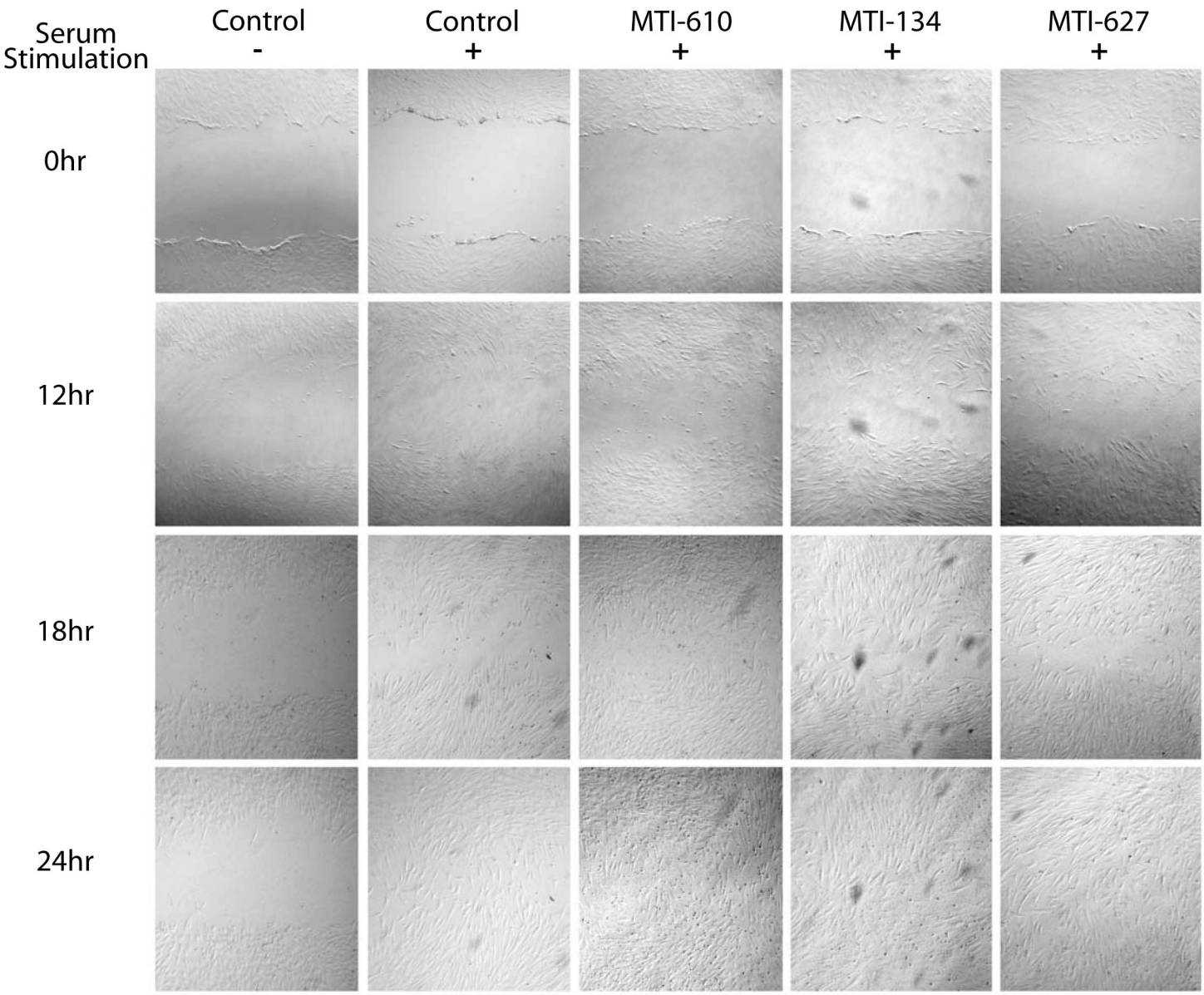

Supplemental Figure 10. Scratch wound assay following serum stimulation in control and patient fibroblast lines. At time 0hr, the wound is similar in all five samples. Without serum, all samples fail to show migration into the wound over 24 hrs (shown only for control), whereas serum addition is associated with appreciable numbers of cells moving into the wounded area. MTI-620, MTI-134 an MTI-627 fibroblasts show healing with comparable dynamics in the presence of serum.

Supplemental Table 1.

Clinical findings of patients with *INPP5E* mutations							
Demographic information							
Family ID	MTI-007	MTI-008	MTI-134	MTI-610	MTI-627	COR-10	COR-21
Country of origin	UAE	UAE	UAE	Turkish	Egyptian	Italian	Italian
Patient	Five affecteds (1 died)	Four affecteds	One affected	Two affecteds	Three affecteds (1 died)	Two affecteds	One affected
Death	Y	N	N	N	Y	N	N
Documented consanguinity	Y	Y	Y	Y	Y	Y	Y
Genetic results							
Nucleotide change; amino acid change	c.1537C>T; p.R512W, c.1546C>T; p.R515W	c.1691G>A; p.R563H	c.1537C>T; p.R512W, c.1546C>T; p.R515W	c.1305G>A; p.R435Q	c.1738A>G; p. K580E	c. 1132C>T; p.R378C	c. 1132C>T; p.R378C
Amino acid alteration	Strongly basic to neutral	Strongly basic to weakly basic	Strongly basic to neutral	Strongly basic to neutral	Basic to acidic	Strongly basic to neutral	Strongly basic to neutral
Exon	7	9	7	6	9	4	4
Mutation type	Homozygous	Homozygous	Homozygous	Homozygous	Homozygous	Homozygous	Homozygous
Neurological signs							
Hypotonia/ataxia	Y	Y	Y	Y	Y	Y	Y
Psychomotor delay	Y	Y	Y	Y	Y	Y	Y
Mental retardation	Y	Y	Y	Y	Y	Y	?
OMA	Y	Y	Y	Y	Y	Y	Y
Breathing abnormalities	N	N	Y	N	N	N	N
Ocular signs							
Retinopathy	Y	Y, Pale optic disc	N	N	N	Y	Y
Coloboma	N	N	N	N	N	N	N
Renal signs							
NPHP/UCD	N	N	N		N	N	N
Kidney ultrasound	Negative	Negative	Negative	Both with bilateral increased echogenicity with cysts	Negative	Negative	Negative
Other organs							
Liver abnormalities	N	N	N	N	Both with elevated transaminases and fibrosis	N	Elevated transaminases with fibrosis/cirrhosis
Polydactyly	N	N	N	N	N	N	N
MRI reading							
MTS	Y	Y	Y	Y	Y	Y	Y
Other abnormalities	-	Plagiocephaly	-	Microcephaly			
Legend: ERG - electroretinogram, MTS - Molar tooth sign, NPHP - nephronophthisis, OMA - Oculomotor apraxia, UCD - urinary concentrating defect.							

Supplemental Table 1. Clinical and molecular findings of patients with *INPP5E* mutations.

Supplemental Table 2.

Mutant haplotype at 9q34.3					
			Families		
SNP	MTI-007	MTI-008	MTI-134	MTI-610	MTI-627
rs1220789			AB		
rs1054879			B		
rs818053			B		
rs818052			A		
rs735107			A		
rs10901140			A		
rs565325			B		
rs456396			B		
rs215156			B		
rs886017			A	AB	
rs12335			A	A	
rs1611122			B	A	AB
rs886112			B	A	B
rs7023064			B	B	B
rs877954			B	A	A
rs3132332	AB		B	A	A
rs2989726	B	AB	B	A	B
rs4641145	B	A	B	B	B
rs914400	B	B	B	A	B
rs705670	A	A	A	A	A
rs710411	A	AB	A	A	A
rs945383	B	AB	B	B	B
rs908831	A	AB	A	A	A
rs1018330	A	AB	A	A	A
rs7028989	B	B	B	B	B
rs7860423	B	B	B	B	B
rs766374	A	AB	A	A	A

Supplemental Table 2. Genotypes for affected individuals within JBTS1-linked families surrounding the candidate interval. Red = recombination events from each family linking to the candidate interval. INPP5E is located between rs705670 and rs710411 (yellow). A block of heterozygosity was detected within the candidate interval in family MTI-008, but it was not possible to detect which of the two remaining linked blocks contained the gene of interest.

Supplemental Table 3.

Marker	Gene	Base Position (UCSC March 2006 Freeze)	Screening Method	Families Screened
D9S1826				
	RXRA	136,438,249	Seq	007, 008
	COL5A1	136,673,473	SSCP and Seq	007, 008
	FCN2	136,912,479		
	FCN1	136,941,255	SSCP	007, 008
	OLFM1	137,106,992	Seq	007, 008, 134, COR10
	C9orf62	137,374,916	SSCP	007, 008
	KIAA0649	137,511,469	SSCP and Seq	007, 008
	C9orf116	137,526,847		
	MRPS2	137,532,375	SSCP and Seq	007, 008
	LCN1	137,553,107	Seq	007, 008
	OBP2A	137,577,806	Seq	007, 008
	PAEP	137,593,425	Seq	007, 008
	GLT6D1	137,655,323	Seq	007, 008, 134, COR10
	LCN9	137,694,989		
	SOHLH1	137,725,076		
	KCNT1	137,733,859	SSCP	007, 008
	CAMSAP1	137,841,248	Seq	007, 008, 134, COR10
	UBADC1	137,956,367	Seq	007, 008, 134, COR10
	BTBD14A	138,043,024	SSCP	
	AK023162	138,146,248		
	LHX3	138,227,917	SSCP and Seq	007, 008
	QSCN6L1	138,238,004	Seq	007, 008, 134, COR10
	GPSM1	138,341,753	Seq	007, 008, 134, COR10
	LOC728489	138,376,173	Seq	007, 008, 134, COR10
	CARD9	138,377,262	SSCP and Seq	007, 008, 134, COR10
	SNAPC4	138,389,850	Seq	007, 008, 134, COR10
	SDCCAG3	138,416,195	Seq	007, 008, 134, COR10
	PMPCA	138,421,822	Seq	007, 008, 134, COR10
	INPP5E	**138,442,893**		
	KIAA0310	138,454,369	Seq	007, 008, 134, COR10
	C9orf163	138,497,768	Seq	007, 008, 134, COR10
	NOTCH1	138,508,717	SSCP and Seq	007, 008, 134, COR10
	EGFL7	138,673,129	SSCP and Seq	007, 008
	AGPAT2	138,687,416	SSCP and Seq	007, 008
	FAM69B	138,726,851		
	AK054908	138,735,639		
	LCN6/LCN10	138,752,440		
	TMEM141	138,805,628		
	KIAA1984	138,810,623	SSCP	007, 008
	pp8875	138,822,013	SSCP	007, 008
	LOC389813	138,858,688		
	PHPT1	138,862,255	SSCP	007, 008
	MAMDC4	138,866,640		
	EDF1	138,876,392	SSCP	007, 008
	TRAF2	138,900,786	SSCP	007, 008
	FBXW5	138,954,708	Seq	007, 008, 134, COR10

Supplemental Table 3. Candidate genes within the JBTS1 locus, delineated by the flanking markers D9S1826 and D9S1838. Base position indicated by UCSC Genome Browser March 2006 freeze. Screening method (SSCP vs. sequence vs. both) for each gene screened is indicated. Families used in the screening are indicated in the last column.

Supplemental Table 3 (continued).

Marker	Gene	Base Position (UCSC March 2006 Freeze)	Screening Method	Families Screened
	C8G	138,959,534	SSCP and Seq	007, 008
	LCN12	138,966,593	SSCP and Seq	007, 008
	PTGDS	138,990,822	SSCP and Seq	007, 008
	FLJ45224	138,996,177		
	C9orf142	139,006,691		
	CLIC3	139,008,881	SSCP	007, 008
	ABCA2	139,021,507	SSCP and Seq	007, 008
	C9orf139	139,041,737		
	FUT7	139,044,447	SSCP and Seq	007, 008
	NPDC1	139,051,882	SSCP and Seq	007, 008
	ENTPD2	139,062,374	SSCP and Seq	007, 008
	C9orf140	139,076,595		
	DKFZp762I052	139,092,017		
	UNQ747	139,101,200	SSCP and Seq	007, 008
	DPP7	139,124,813		
	GRIN1	139,153,430		
	LOC389816	139,183,033		
	ANAPC2	139,189,057	Seq	007, 008, 134, COR10
	SSNA1	139,202,954		
	C9orf75	139,205,890		
	MGC14327	139,218,356		
	NDOR1	139,220,004	Seq	007, 008, 134, COR10
	RNF208	139,234,528		
	MGC59937	139,239,465	Seq	
	SLC34A3	139,245,030	Seq	007, 008, 134, COR10
	TUBB2C	139,255,532	Seq	007, 008, 134, COR10
	LOC401565	139,257,858		
	LOC441476	139,265,551		
	COBRA1	139,269,768	Seq	007, 008, 134, COR10
	C9orf167	139,292,101	Seq	
	MGC61598	139,314,755		
	FLJ20433	139,321,178	Seq	007, 008, 134, COR10
	NOXA1	139,437,668	Seq	007, 008, 134, COR10
	ENTPD8	139,448,637	Seq	007, 008, 134, COR10
	NELF	139,462,498	Seq	007, 008, 134, COR10
	PNPLA7	139,474,226		
	MRPL41	139,566,165		
	WDR85	139,569,182		
	ZMYND19	139,596,352	SSCP and Seq	007, 008
	ARRDC1	139,619,917		
	C9orf37	139,629,610	SSCP and Seq	007, 008
	EHMT1	139,633,265	SSCP and Seq	007, 008
D9S1838				